doi:10.1016/j.jmb.2005.09.047 J. Mol. Biol. (2005) 354, 385–402

JMB

Available online at www.sciencedirect.com

SCIENCE DIRECT®

ELSEVIER

Versatile Peroxidase Oxidation of High Redox Potential Aromatic Compounds: Site-directed Mutagenesis, Spectroscopic and Crystallographic Investigation of Three Long-range Electron Transfer Pathways

Marta Pérez-Boada[1]†, Francisco J. Ruiz-Dueñas[1]†, Rebecca Pogni[2] Riccardo Basosi[2], Thomas Choinowski[3] María Jesús Martínez[1], Klaus Piontek[3] and Angel T. Martínez[1]*

[1]*Centro de Investigaciones Biológicas, CSIC, Ramiro de Maeztu 9, E-28040 Madrid Spain*

[2]*Department of Chemistry University of Siena, via Aldo Moro, I-53100 Siena, Italy*

[3]*Institute of Biochemistry Swiss Federal Institute of Technology (ETH) Schafmattstrasse 18 (HPM) ETH Hönggerberg, CH-8093 Zürich, Switzerland*

Versatile peroxidases (VP), a recently described family of ligninolytic peroxidases, show a hybrid molecular architecture combining different oxidation sites connected to the heme cofactor. High-resolution crystal structures as well as homology models of VP isoenzymes from the fungus *Pleurotus eryngii* revealed three possibilities for long-range electron transfer for the oxidation of high redox potential aromatic compounds. The possible pathways would start either at Trp164 or His232 of isoenzyme VPL, and at His82 or Trp170 of isoenzyme VPS1. These residues are exposed, and less than 11 Å apart from the heme. With the purpose of investigating their functionality, two single mutations (W164S and H232F) and one double mutation (W164S/P76H) were introduced in VPL that: (i) removed the two pathways in this isoenzyme; and (ii) incorporated the absent putative pathway. Analysis of the variants showed that Trp164 is required for oxidation of two high redox potential model substrates (veratryl alcohol and Reactive Black 5), whereas the two other pathways (starting at His232 and His82) are not involved in long-range electron transfer (LRET). None of the mutations affected Mn^{2+} oxidation, which would take place at the opposite side of the enzyme. Substitution of Trp164 by His also resulted in an inactive variant, indicating that an indole side-chain is required for activity. It is proposed that substrate oxidation occurs *via* a protein-based radical. For the first time in a ligninolytic peroxidase such an intermediate species could be detected by low-temperature electron paramagnetic resonance of H_2O_2-activated VP, and was found to exist at Trp164 as a neutral radical. The H_2O_2-activated VP was self-reduced in the absence of reducing substrates. Trp164 is also involved in this reaction, which in the W164S variant was blocked at the level of compound II. When analyzing VP crystal structures close to atomic resolution, no hydroxylation of the Trp164 C^{β} atom was observed (even after addition of several equivalents of H_2O_2). This is in contrast to lignin peroxidase Trp171. Analysis of the crystal structures of both peroxidases showed differences in the environment of the protein radical-forming residue that could affect its

† M.P.-B. and F.J.R.-D. contributed equally to this work.

Abbreviations used: CCP, cytochrome *c* peroxidase; CIP, *Coprinopsis cinerea* peroxidase; DFT, density functional theory; DHP, dehydrogenation polymer; ENDOR, electron nuclear double resonance; EPR, electron paramagnetic resonance; KTBA, α-keto-γ-thiomethylbutyric acid; LiP, lignin peroxidase; LRET, long-range electron transfer; MnP, manganese peroxidase; NBS, *N*-bromosuccinimide; rms, root-mean-square; SLS, Swiss Light Source; VP, versatile peroxidase; VP*, recombinant VP.

E-mail address of the corresponding author: atmartinez@cib.csic.es

reactivity. These variations would also explain differences found for the oxidation of some high redox potential aromatic substrates.

Keywords: versatile peroxidase; high redox potential aromatic substrates; long-range electron transfer; tryptophan radical; site-directed mutagenesis

*Corresponding author

Introduction

Long-range electron transfer (LRET) has been reported to be operative in redox proteins, like cytochrome *c* peroxidase (CCP). This heme-containing enzyme oxidizes cytochrome *c* at the protein surface and transfers electrons to a stable Trp radical situated near the heme cofactor *via* three amino acid residues.[1,2] Intramolecular LRET also occurs in a few other proteins, like DNA photolyase whose flavin cofactor is reduced by a Trp residue in an electron transfer pathway that includes two other aromatic amino acid residues.[3] LRET has been suggested to be involved also in lignin biodegradation brought about by ligninolytic heme peroxidases secreted by fungi from the group of white-rot basidiomycetes. These enzymes catalyze the oxidative degradation of lignin by H_2O_2, a key step of the carbon cycle in terrestrial ecosystems.[4] LRET in lignin biodegradation would include electron transfer both: (i) in the peroxidase molecule, to overcome steric hindrances preventing the access of lignin to the heme cofactor; and (ii) in the lignin macromolecule itself resulting in breakdown of the most labile inter-unit linkages at some distance from the enzyme.[5,6] Due to the high redox potential required for lignin oxidation, ligninolytic peroxidases have been the object of high interest as industrial biocatalysts.

The molecular structure of ligninolytic peroxidases includes a heme cofactor located at an internal cavity (the "heme pocket") connected to the protein surface by two small access channels.[7–10] The larger one is conserved in all heme peroxidases and is used by hydrogen peroxide to reach the heme and react with Fe^{3+} forming the two-electron activated form of the enzyme (called compound I). Moreover, the entrance of this channel forms the substrate-binding site in some peroxidases, e.g. horseradish peroxidase. The second channel extends directly to the heme propionates being the site where some specialized ligninolytic peroxidases oxidize Mn^{2+} to Mn^{3+}. The latter acts as a diffusible oxidizer on phenolic lignin and other organic molecules. Oxidation of aromatic compounds has been widely studied in heme peroxidases from class III (plant peroxidases) and also from class II (fungal peroxidases).[8] The classical hypothesis that the reaction would take place in the vicinity of the heme has been demonstrated for several plant peroxidases and for the peroxidase from the saprophytic fungus *Coprinopsis cinerea* (synonym *Coprinus cinereus*) (CIP).[11,12] However, no crystal structure of a ligninolytic peroxidase in complex with an aromatic substrate or substrate analogue has been reported up to date. It is generally accepted that the narrow heme channel prevents the direct contact between the large lignin polymer and the heme. This implied the involvement of low molecular mass compounds as peroxidase redox mediators, like the fungal metabolite 3,4-dimethoxybenzyl alcohol (veratryl alcohol).[13] However, even such small compounds seem to be too large to approach the heme through the above-mentioned channel(s). Therefore, LRET from the surface of the enzyme to the heme cofactor represents a reasonable alternative to explain oxidation of redox mediators, aromatic substrates, and even polymeric lignin.[6,14–17]

Versatile peroxidase (VP) has been recently described as a new family of ligninolytic peroxidases, together with lignin-peroxidase (LiP) and manganese peroxidase (MnP) both reported for *Phanerochaete chrysosporium* for the first time.[7] The complete genome of this model fungus has been recently sequenced revealing two families of LiP and MnP genes together with a "hybrid peroxidase" gene.[18] However, the sequence of the latter gene is more related to non-ligninolytic CIP[19] than to VP. Up to date, VP seems to be produced only by fungi from the genera *Pleurotus*, *Bjerkandera* and *Lepista*,[20–27] and maybe also by *Panus* and *Trametes* species.[7,28] This fourth fungal peroxidase family should be included in peroxidase class II,[29] together with the MnP, LiP and CIP families. The most noteworthy aspect of VP is that it combines the substrate specificity characteristics of the three other fungal peroxidase families. In this way, it is able to oxidize a variety of (high and low redox potential) substrates including Mn^{2+}, phenolic and non-phenolic lignin dimers, α-keto-γ-thiomethylbutyric acid (KTBA), veratryl alcohol, dimethoxybenzenes, different types of dyes, substituted phenols and hydroquinones.[30,31]

VP genes (and cDNA) were first cloned and sequenced from *Pleurotus eryngii* in 1999–2000,[22,32] and recently from *Lepista irina*,[27] and *Bjerkandera* sp. (GenBank code AY217015; unpublished work). It was suggested that the catalytic properties of the new peroxidases were due to a hybrid molecular architecture combining different substrate binding and oxidation sites.[33] Recently, VP from *P. eryngii* was investigated using several techniques in order to understand the structural and functional peculiarities of this new peroxidase family. Here, we address the most important aspects of ligninolytic peroxidase activity, i.e. the identification of the aromatic substrate-binding site as well as how

oxidation of high redox-potential aromatic compounds occurs. The crystal structure of wild-type and native recombinant (non-glycosylated) *P. eryngii* VP has been recently determined at high resolution. In addition crystal structures of several VP preparations and site-directed mutagenesis variants were determined (Piontek *et al.*, unpublished results). Two of these structures are analyzed here contributing to the understanding of the mechanism of aromatic substrate oxidation in VP. During the analysis of VP crystal structures and molecular models, three possible LRET pathways were identified that were investigated by site-directed mutagenesis. Simultaneously, low temperature electron paramagnetic resonance (EPR) measurements showed the formation of a protein-based radical after VP activation by H_2O_2. Finally, the effect of VP site-directed mutagenesis and peroxide treatment were investigated in two crystal structures. The results obtained provide the first structure–function information about aromatic substrate oxidation by a member of the VP family, and can also relate to the understanding of some aspects of the mechanisms of high-redox potential substrate oxidation in other peroxidases.

Results

VP catalytic cycle and spontaneous decay of compounds I and II

Recombinant VP (VP*) was obtained by heterologous expression in *Escherichia coli* W3110 transformed with the cDNA encoding the mature isoenzyme VPL, and *in vitro* activation (in the presence of the cofactor) of the VP* protein, which formed inclusion bodies as shown by SDS-PAGE after cell lysis and centrifugation separation.[34] One step purification using anion exchange chromatography resulted in electrophoretically homogeneous protein.

A catalytic cycle (Figure 1(a)) that combines the cycles of other fungal peroxidases, including LiP and MnP, was proposed by Ruiz-Dueñas *et al.*[22] The basic features are common to most peroxidases, but VP is unique regarding the substrates that it is able to oxidize. Transient states in the catalytic cycle were studied using veratryl alcohol as the reducing substrate. Reaction of the ferric resting enzyme with one molecule of H_2O_2 resulted in spectral changes that suggested formation of compound I, a Fe^{4+}-oxo·porphyrin$^{\cdot+}$ complex.[35] Compound I oxidizes a molecule of veratryl alcohol with spectral changes, suggesting formation of compound II (Fe^{4+}-oxo). This intermediate would oxidize a second veratryl alcohol molecule while being reduced back to the resting state. In addition to veratryl alcohol (the typical LiP substrate) VP* can also oxidize high redox potential dyes, such as Reactive Black 5, as well as low redox potential dyes, substituted phenols and Mn^{2+}, as reported for the wild-type (non-recombinant) fungal enzyme.[31]

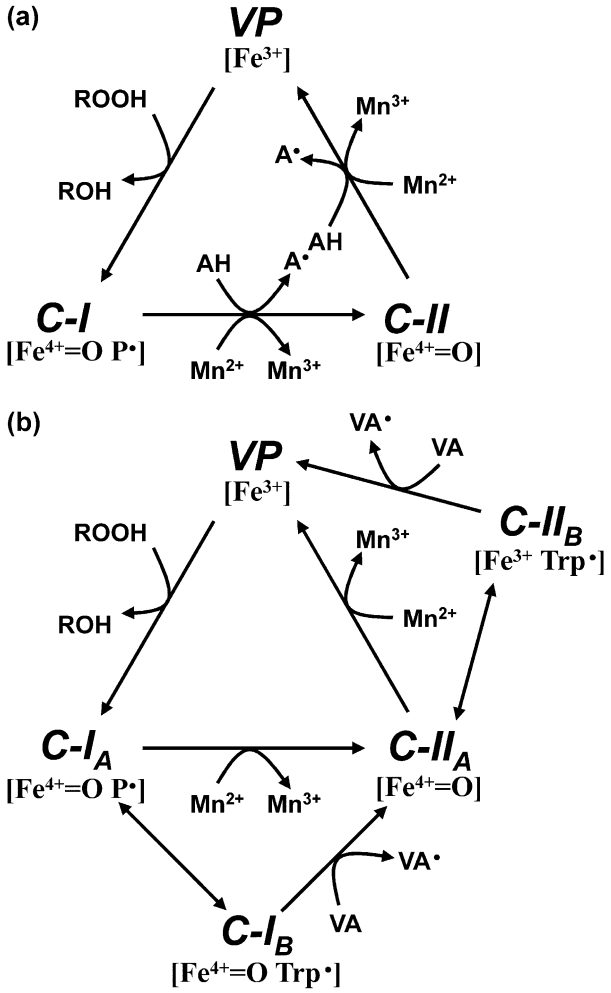

Figure 1. Schemes of VP catalytic cycle. (a) Basic cycle described by Ruiz-Dueñas *et al.*[22] including two-electron oxidation of the resting peroxidase (VP, containing Fe^{3+}) by hydroperoxide to yield compound I (C-I, containing Fe^{4+}-oxo and porphyrin cation radical), whose reduction in two one-electron reactions results in the intermediate compound II (C-II, containing Fe^{4+}-oxo after porphyrin reduction) and then the resting form of the enzyme. As shown in the cycle, VP can oxidize both: (i) aromatic substrates (AH) to the corresponding radicals (A·); and (ii) Mn^{2+} to Mn^{3+}, the latter acting as a diffusible oxidizer. (b) Extended cycle including also compounds I_B (C-I_B, containing Fe^{4+}-oxo and Trp radical) and II_B (C-II_B, containing Fe^{3+} and Trp radical) involved in oxidation of veratryl alcohol (VA) and other high redox potential aromatic compounds (C-I_B and C-II_B are in equilibrium with C-I_A and C-II_A respectively, which correspond to C-I and C-II in (a) (other low redox potential aromatic compounds are probably oxidized by both the A and B forms but they are not included for simplicity). The active Trp in C-I_B and C-II_B would be Trp164 (the part of the cycle showing aromatic substrate oxidation would be also applicable to LiP, being Trp171 the active amino acid).

Resting VP shows a typical peroxidase spectrum,[35] characterized by the Soret band at 407 nm,

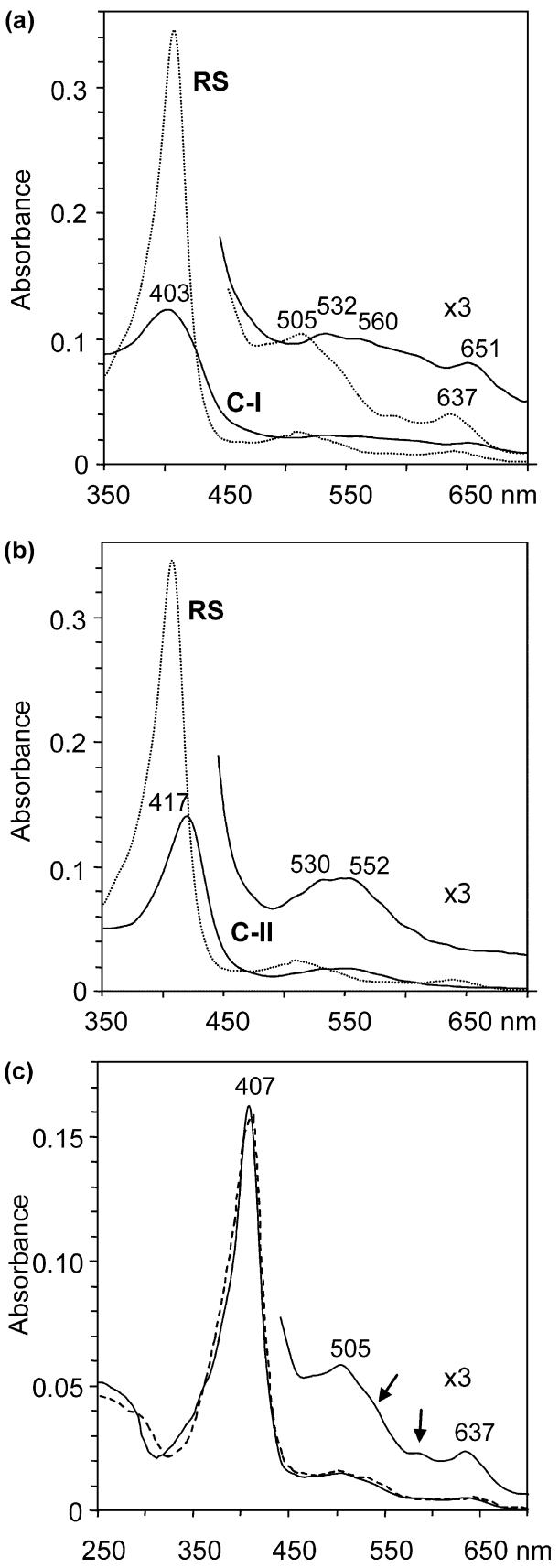

Figure 2. Different electronic absorption spectra of VP and its W164S variant. (a) Spectra of the resting state (RS) of VP* (dotted line) and compound I (continuous line) formed by addition of one equivalent of H_2O_2 in 10 mM sodium tartrate(pH 5) (details of the 450 nm–700 nm region are shown in ×3 scale). (b) Spectra of the VP compound II (continuous line) observed after addition to the resting state (dotted line) of two equivalents of H_2O_2 in 10 mM sodium tartrate (pH 5) (details of the 450 nm–700 nm region of compound II spectrum are shown in ×3 scale). (c) Comparison of the resting state spectra of the W164S variant (continuous line) and native VP* (broken line).

and charge transfer bands at 505 nm (CT2) and 637 nm (CT1) (two minor α and β additional bands are indicated with arrows) (Figure 2). In the spectrum of compound I (Figure 2(a)) obtained after adding one H_2O_2 equivalent to the resting enzyme, the Soret band was lowered and displaced to 403 nm, and small bands were observed at 532 nm (β), 560 nm (α) and 651 nm (CT1). In the absence of enzyme-reducing substrates, VP* compound II could be observed after adding two equivalents of H_2O_2 to the resting enzyme, as described for LiP and MnP.[36,37] Its spectrum (Figure 2(b)) includes an opposite displacement of the Soret band to 417 nm, and small bands at 530 nm (β) and 552 nm (α). Since the redox state of the iron is not modified the latter changes are ascribed to the reduction of a porphyrin cation radical.

Formation of the VP* transient states was studied using stopped-flow techniques at different pH values. Figure 3(a) shows compound I formation by addition of one equivalent of H_2O_2 to resting VP* (down arrow) and its reduction by veratryl alcohol (up arrow) passing through compound II, as evidenced by the shoulder around 420 nm. The kinetics of compounds I and II formation, measured at the corresponding isosbestic points, is illustrated in Figure 3(a) (inset). Whereas compound I formation was independent of pH (in the range of pH 3.5–pH 7) with a k_1 value of $4.1\times10^6\,M^{-1}\,s^{-1}$, reduction of compounds I and II by veratryl alcohol was strongly dependent on pH (Table 1). Analysis of VP* turnover showed that reduction of the H_2O_2-activated enzyme is produced not only in the presence of veratryl alcohol (or other enzyme substrates) but also in absence of any VP* substrate (Figure 3(b)). However, the self-reduction rates are lower than found in the presence of a reducing substrate (Figure 3(b), inset). These results suggest the existence of an efficient protein intramolecular reductant.

Production and steady-state kinetics of W164S, W164H, P76H, H232F and W164S/P76H variants

The heterologous expression system and *in vitro* activation procedure used to obtain native VP* were also applied to the site-directed mutagenesis variants designed to investigate the mechanism of oxidation of high redox potential compounds. In all cases each VP* variant was the major protein found after SDS-PAGE of the material recovered from

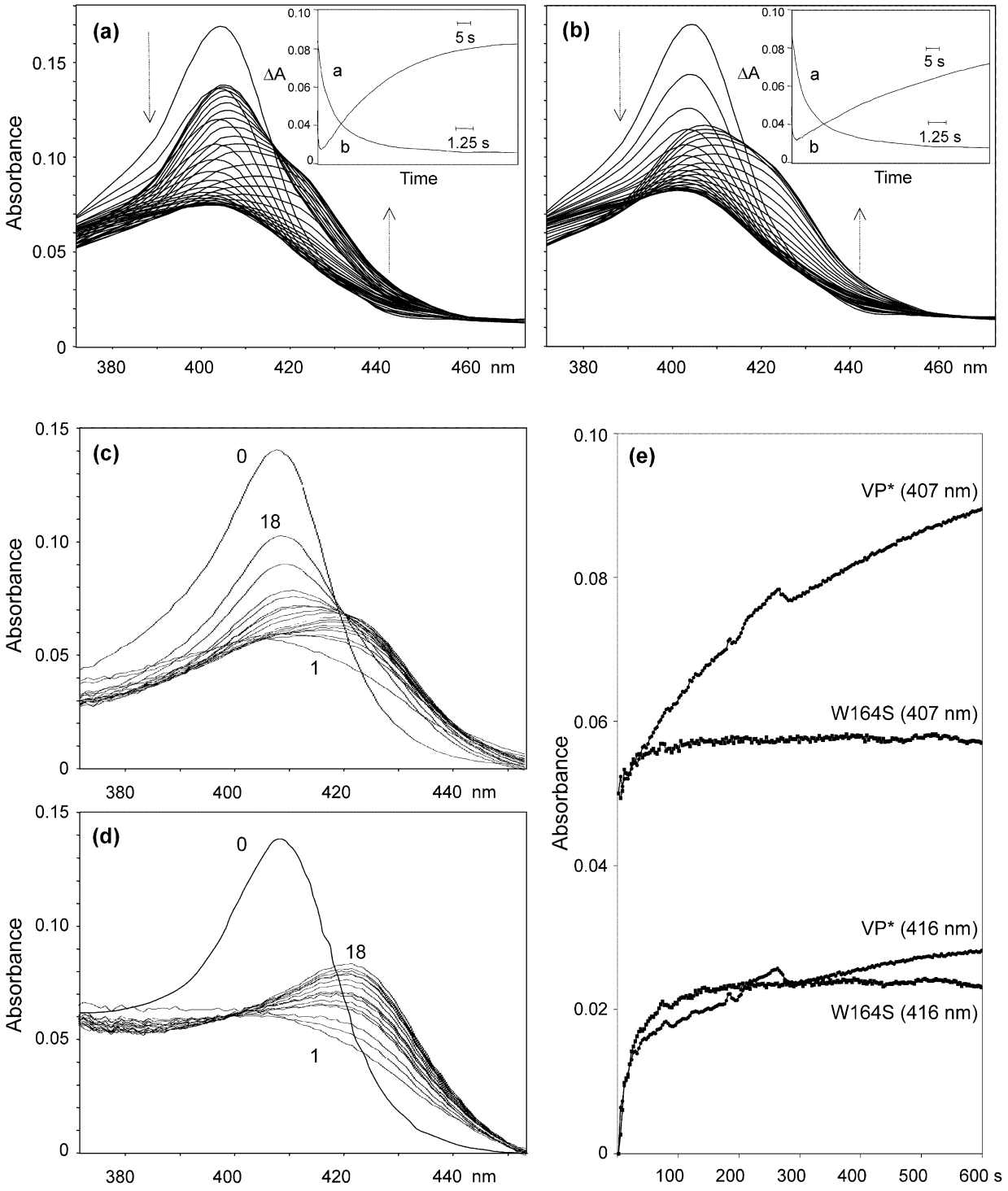

Figure 3. Turnover studies of native VP* and its W164S variant. (a) and (b), Rapid kinetics of native VP* turnover in the presence (a) and absence (b) of veratryl alcohol (stopped-flow rapid scan diode array spectra). Spectra were recorded at 24 °C during 170 s, after mixing 3 μM VPL* in citrate-phosphate-sulfate buffer (μ = 50 mM, pH 4.5) with one equivalent of H_2O_2, in the presence or in the absence of 100 mM VA (the same number of spectra are shown in (a) and (b) using a logarithmic time scale). The arrows indicate the decrease and increase of absorbance during formation of compound I and II, respectively. The insets show formation of compound I at 397 nm (a) and compound II at 416 nm (b) against time, under both conditions. Compound II was partially reduced back to resting enzyme (407 nm), especially in the presence of veratryl alcohol, although VP turnover was not completed in the present time scale and experimental conditions. (c) to (e), Diode array spectra of compound I formation and self-reduction in native VP (c) and its W164S variant (d) (long term incubation for 10 min). Changes in the whole spectrum (375 nm–475 nm region) and absorbance traces at 416 nm and 407 nm showing reduction to compound II and resting enzyme respectively (e), are presented. Compound I was obtained by adding one equivalent of H_2O_2 to VP* (1 μM) and its self-reduction was followed at 24 °C. Traces 1–18 (in (c) and (d)) correspond respectively to 2, 5, 8, 11, 14, 17, 20, 23, 26, 29, 45, 60, 75, 90, 120, 150, 300 and 600 s (trace 0 shows the VP* spectrum before H_2O_2 addition).

Table 1. Kinetic constants for VP* compounds I (k_2) and II (k_3) reduction by veratryl alcohol

pH	k_2 ($M^{-1}\,s^{-1}$)	k_3 ($M^{-1}\,s^{-1}$)
3.5	1300±200	300±150
4.5	350±110	93±2
5.5	72±2	–

Means and 95% confidence limits at different pH values obtained by one-step mixing turnover method using native VPL*.

inclusion bodies. The yield of conversion of this material into active enzyme was similar or in some cases better than found for native VP*, with up to 10% *in vitro* activation. The purified variants migrated at the same distances as the native VP* which corresponded to a molecular mass similar to that of deglycosylated wild-type fungal peroxidase (~38 kDa).

Kinetic characterization of the site-directed mutagenesis variants was accomplished by measuring the initial oxidation rates of three representative VP substrates, namely veratryl alcohol, Reactive Black 5, and Mn^{2+}, and were compared with the rates of native VP*. Veratryl alcohol is a non-phenolic (high redox potential) aromatic compound oxidized by LiP and VP to its cation radical. A role either as a redox mediator or as a kind of "cofactor" has been proposed.[38] VP also presents high affinity for several high redox potential dyes like Reactive Black 5,[39,40] which are decolorized by the enzyme at a low rate but with a catalytic efficiency comparable with that of Mn^{2+} oxidation. The latter cation is the typical substrate of MnP, but can be also oxidized by VP with high efficiency.[39]

Table 2 shows the apparent kinetic constants of the different variants obtained compared with the native VP*, and the wild-type (fungal) enzyme. The kinetic constants of the recombinant enzyme expressed in *E. coli* were in general similar to those of the wild-type VP purified from cultures of *P. eryngii*, although it showed lower affinity for Mn^{2+}, suggesting that the carbohydrate moiety (absent from bacterial VP*) contributed to the binding of this cation. The lack of glycosylation also results in lower temperature stability (data not shown). All the site-directed mutagenesis variants, where Trp164 had been substituted either by Ser or His, were completely unable to oxidize both veratryl, alcohol and Reactive Black 5. The double mutant W164S/P76H exhibited the same behavior as the single mutants W164S and W164H. On the other hand, the efficiency (k_{cat}/K_m) of the H232F and P76H variants oxidizing veratryl alcohol was increased slightly, whereas the efficiency of the H232F variant oxidizing Reactive Black 5 was decreased. Finally, the apparent K_m and k_{cat} values for the oxidation of Mn^{2+} were similar for the native VP* and the site-directed mutagenesis variants.

Spectroscopic measurements of native VP* and its W164S variant

The electronic absorption spectra of all the obtained VP* variants presented, at the resting state, the sharp Soret band around 407 nm, and the bands at 505 nm and 637 nm in the visible region, characteristic of the native VP* spectrum (as shown in Figure 2(c) for the W164S variant). This suggests that the substitutions introduced (Ser for Trp164, His for Trp164 and Pro72, and Phe for His232) did not produce any significant change in the heme environment.

Veratryl alcohol did not speed up the turnover of the W164S variant, in contrast with that previously shown for the native VP* using rapid spectrophotometry. Moreover, the spontaneous decay of the H_2O_2-activated VP* to the resting state was blocked by the substitution of Trp164. Figure 3(c)–(d) compares self-reduction of compound I including the initial spectrum before addition of one equivalent of H_2O_2, and those recorded during long-term decay of both native VP* (c) and its W164S variant (d). Individual traces in Figure 3(e) show that Trp164 is absolutely required for compound II self-reduction to the resting enzyme (followed at 407 nm), since this compound

Table 2. Steady-state kinetic constants for oxidation of three substrates by the five site-directed mutagenesis variants compared with native VP*, and wild-type VP produced by *P. eryngii*

		VP[a]	VP*	W164S	W164H	H232F	P76H	W164S/P76H
VA	K_m (μM)	3000	2750	–	–	3580	2410	–
	k_{cat} (s^{-1})	12.9	8.0	0	0	14.0	11.0	0
	k_{cat}/K_m ($s^{-1}\,mM^{-1}$)	4.3	3.0	0	0	4.0	4.4	0
RB5	K_m (μM)	4.0	2.8	–	–	3.6	3.1	–
	k_{cat} (s^{-1})	3.6	5.0	0	0	4.7	6.0	0
	k_{cat}/K_m ($s^{-1}\,mM^{-1}$)	900	1780	0	0	1330	1900	0
Mn^{2+}	K_m (μM)	19	189	110	126	218	262	351
	k_{cat} (s^{-1})	118	298	207	320	308	291	247
	k_{cat}/K_m ($s^{-1}\,mM^{-1}$)	6200	1600	1900	2530	1400	1100	700

The kinetic constants for oxidation of veratryl alcohol (VA), Reactive Black 5 (RB5) and Mn^{2+} by native VP* (allelic variant VPL2) and five variants were calculated from reactions carried out in 100 mM sodium tartrate (pH 3), VA; pH 3.5, RB5; or pH 5, Mn^{2+}) in the presence of 0.1 mM H_2O_2. All the 95% confidence limits obtained were below 10% of the mean values presented.

[a] Wild-type VP (allelic variant VPL2) constants taken from Heinfling *et al.*[31]

accumulated during decay of the W164S variant. However, this is not the case for compound I reduction, since only small differences in the rate of compound II formation (followed at 416 nm) were observed when the W164S variant and the native VP* were compared.

Simultaneously, EPR spectra of VP* were collected (at 20 K). The spectra were run before and after addition of eight equivalents of H_2O_2 to resting VP* in the absence of a reducing substrate. This resulted in compound I formation, as shown by the electronic absorption spectrum (after 10 s). In the first case (Figure 4(a)) the EPR spectrum was dominated by the high-spin Fe^{3+} signal (at $g=6.0$ and 2.0) of the peroxidase resting state (the $g=4.3$ signal corresponds to a non-heme iron impurity). The Fe^{3+} spin state is in agreement with the presence of the CT1 band (637 nm) in the electronic absorption spectrum of VP* (Figure 2(c)), which is assigned to a charge transfer transition from the porphyrin to the iron.[41] After 10 s following H_2O_2 addition and rapid freezing, the ferric high-spin signal strongly decreased, and an intense radical-like new signal appeared (at $g=2.0027$) that would correspond to a protein radical species (Figure 4(b)). This signal did not increase after longer incubation times. Spin quantitation of the narrow radical signal yielded 0.25 spin/heme. A detail of the EPR spectrum of this radical is shown in Figure 4(c), corresponding to an isotropic signal characterized by a doublet with resolved sub-splittings centered at $g=2.0027$. The line shape and the low g_{iso} value of the radical spectrum resembles that reported for other protein-based radicals that most likely corresponds to a Trp free radical.[42,43] The intensity of the protein radical signal strongly decreased at higher temperatures and incubation times.

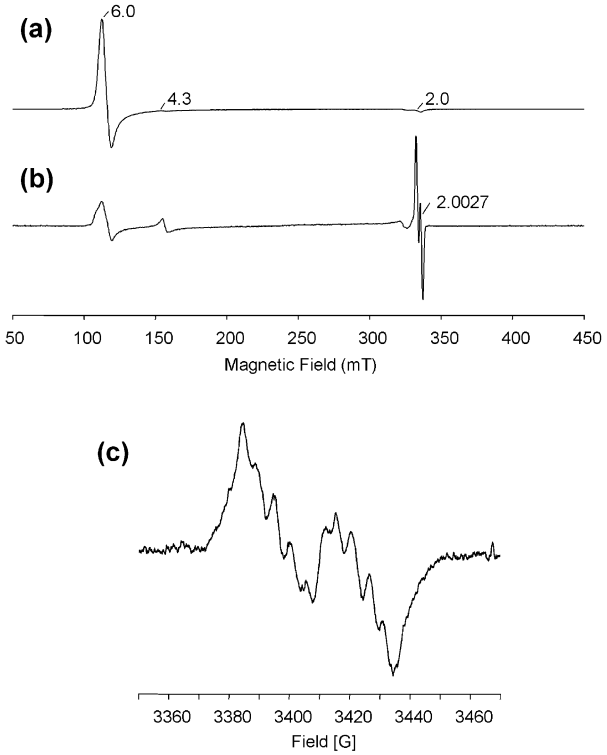

Figure 4. EPR detection of protein radical after H_2O_2 addition to resting VP. X-band EPR spectra of native VP* before (a) and 10 s after addition of eight equivalents of H_2O_2 (b). A detail of the enzyme radical signal is also provided (c). All spectra were recorded at 20 K, $\nu=9.4$ GHz, 2 mW microwave power, and 100 kHz modulation frequency. The modulation amplitude was 10 G in (a) and (b), and 2 G in (c).

Crystallographic analysis of peroxide-treated VP* and W164S variant

Single crystals of native VP*, obtained from protein pretreated with H_2O_2 in order to create the physiological situation when produced by the fungus, and its W164S variant were subject to crystallographic investigations. Both proteins form isomorphous crystals of a bi-pyramidal shape with a size of ca. 300 μm×100 μm×100 μm, and have space group $P4_3$. The data processing and refining statistics showed that the completeness and the overall quality of the data were good. Residues 1 to 319 (H_2O_2-pretreated VP model) or 320 (W164S model) are included together with the heme and several cations (see below). The C-terminal peptide (from residue 320 or 321 to the terminal Ser331) was found to be disordered, indicating a high flexibility in this region. No attempts to build the corresponding amino acids were successful. This was also found in various other VP* variant crystal structures as well as in the crystal structure of wild-type *P. eryngii* VP, which have been recently determined and compared in detail (Piontek *et al.*, unpublished results). Using the micro-focus beam line of the SLS synchrotron, in combination with the good quality of the crystals, well-defined high-resolution structures were obtained.

The overall structures of the native VP*, and its W164S variant are very similar. The rms deviation of the two structures based on C^{α} atoms was about 0.2 Å, with Val289 and Gly224 being the only two residues whose C^{α} positions differ by more than 1 Å. These residues are about 24 Å apart from residue 164, and are situated on two flexible loop regions. The above differences are most likely related to high temperature factors or disorder. The VP* structures include 11 α-helices (Ala12-Asn27, Glu36-Ala49, Ser64-Glu72, Ile81-Lys94, Ala99-Ser112, Val145-Ala155, Pro159-Ile171, Gln196-Glu200, Gln229-Arg236, Ala241-Ser246 and Gln251-Ala266), four disulphide bridges (Cys3-Cys15, Cys14-Cys278, Cys34-Cys114 and Cys242-Cys307) and two structural Ca ions. The Mn-binding site formed by one of the heme propionates and by the carboxylates of Glu36, Glu40 and Asp175 in MnP, was identified as such in the VP* structures. However, only one of the structures (native VP*) showed a Mn^{2+} at this position. Moreover, its coordination was unexpected, since it was located at 1.82 Å from Glu36, 2.08 Å from heme propionate, and 3.08 Å from Asp175

(with water molecules 229, 374 and 56 at 3.6–3.8 Å being too far for a coordination) but Glu40 is not involved. In the W164S variant structure a water molecule occupies exactly the position of Mn^{2+}, since this enzyme was not incubated with a Mn salt.

Two of the putative LRET pathways (see Figure 8(a)) for oxidation of high redox potential aromatic substrates previously suggested by molecular models, were identified in the crystal structures of isoenzyme VPL. Residues homologous to a third pathway (see Figure 8(b)), in the molecular model of a second VP isoenzyme (VPS1), were also identified in the crystal structure. The three putative pathways in VPL are formed by (i) His232-Asp231 *via* backbone atoms and a H-bond from the carboxylate of Asp231 to the side-chain of the proximal His169, (ii) *via* backbone atoms between Trp164 and Leu165 and a van der Waals contact between C^{β} of Leu165 to the methyl-group C of the heme, and (iii) Pro/His76-Ala77–Asn78 *via* backbone atoms and a H-bond from the side-chain oxygen atom of Asn78 to the distal His47. The linear distances to the heme carbon atoms are 10.48 Å from C^{α} of His232 to the methyl group of pyrrol-B, 8.22 Å from C^{α} of Trp164 to the methyl group of pyrrol-C, and 10.51 Å from C^{α} of Pro76 to the methyl group of pyrrol-A. The above-described site-directed mutagenesis investigations of the three pathways, show unambiguously (see Table 2) that only the Trp164 pathway is involved in oxidation of veratryl alcohol and Reactive Black 5 by VP. Therefore, the subsequent crystallographic analyses focused on this pathway and the environment of the exposed Trp residue.

A noteworthy finding was the lack of any indication of hydroxylation at the C^{β} of Trp164 of the native VP* that had been treated with several equivalents of H_2O_2. In other words there was no significant electron density in the crystal structure found (Figure 5). This was also true for the "pristine" native VP*, which had never been in contact with peroxide and the W164S variant, as well as for the wild-type fungal VP (data not shown). This contrasts with results obtained with *P. chrysosporium* LiP as discussed below. During oxidation of veratryl alcohol, Reactive Black 5, and other high redox potential substrates, electrons would travel from VP* Trp164 side-chain to the backbone, and then to the side-chain of the adjacent Leu165, whose C^{β} is at 3.66 Å from the carbon of methyl-C of heme (2.37 Å hydrogen distance) (Figure 6). Comparison with LiP isoenzymes shows either Met (LiPH8) or Leu (LiPH2) at the

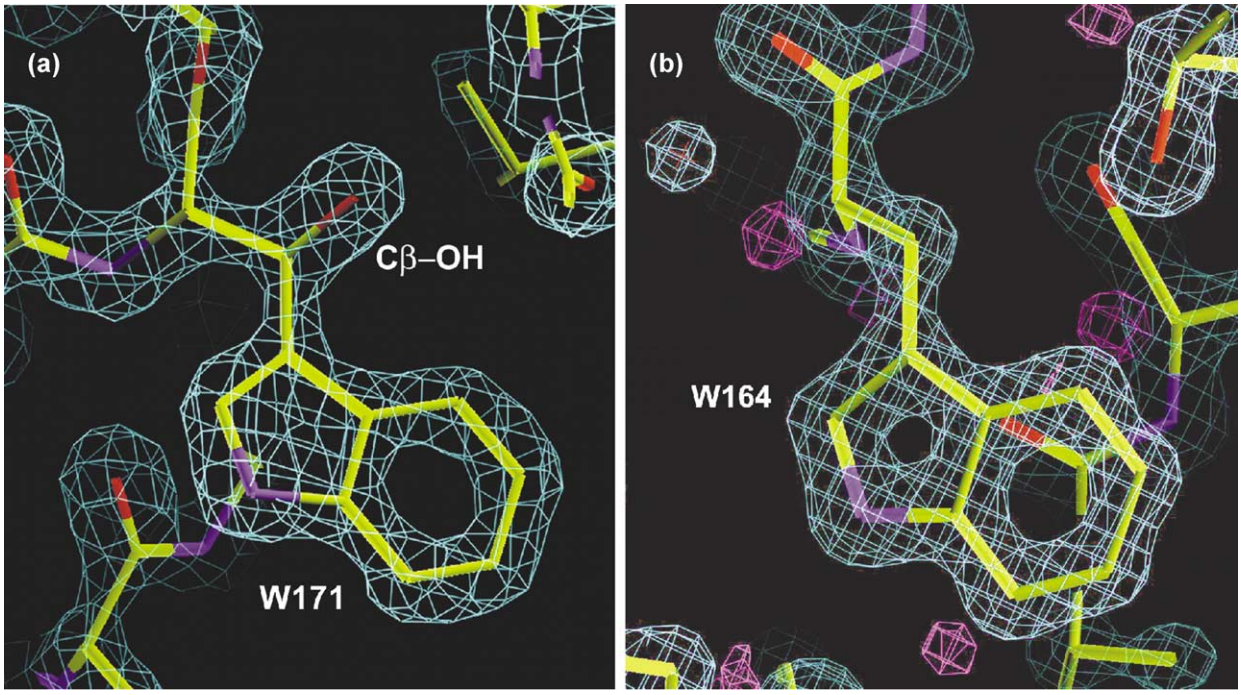

Figure 5. (a) Hydroxylation of the Trp171 C^{β} in the crystal structure of wild-type LiP-H8 at 1.70 Å, and (b) absence of Trp164 hydroxylation in the VP* crystal structure at 1.33 Å. Pristine VP* expressed *E. coli* and activated *in vitro*, was treated with six equivalents of H_2O_2 in the absence of reducing substrates, crystallized, and analyzed by X-ray diffraction (PDB entry 2BOQ). LiP-H8 was obtained from *P. chrysosporium*, crystallized and its crystal structure determined (PDB entry 1LLP). Since this fungus has a H_2O_2-producing system, the crystallized enzyme had reacted with H_2O_2, and C^{β}-hydroxylation was produced.[59,60] In (b) a $(2F_o-F_c)$ electron density map contoured at 2.5σ is depicted in cyan and a (F_o-F_c) electron density map contoured at the 1.5σ level is shown in magenta. No indication is found for an electron density, which could correspond to a putative hydroxyl group at the C^{β} of Trp164. Only residual difference electron density can be seen close to some C atoms, most likely resulting from H-atom contributions. In (a) A $(2F_o-F_c)$ electron density map at the 2.5σ contour level. The O atom of the C^{β}-hydroxyl group was omitted for phase calculation. Nevertheless, the density corresponding to the hydroxyl group is clearly visible.

homologous VP Leu165 position. Eight neighbor residues, only three of them conserved, are shown to illustrate the differences between both structures, as well as the position of the proximal histidine residues, whose N^{ϵ} atom acts as ligand of heme iron at 2.11 Å in VP and 2.15 Å in LiP (see Figure 6).

The crystal structure of the W164S variant was compared with the native enzyme to identify any modification caused by the mutation introduced. A superposition of the mutated area in both proteins, where a Ser residue occupies the position of Trp164, is shown in Figure 7. The Ser side-chain occupies two equally probable positions in the crystal structure. All side-chains of the residues adjacent to the mutated Trp stayed in similar positions after the mutation except for Glu243 and especially Arg257. Elimination of the bulky Trp indole moiety allowed the movement of the side-chain of this Arg residue towards the position previously occupied by Trp164 forming now a new

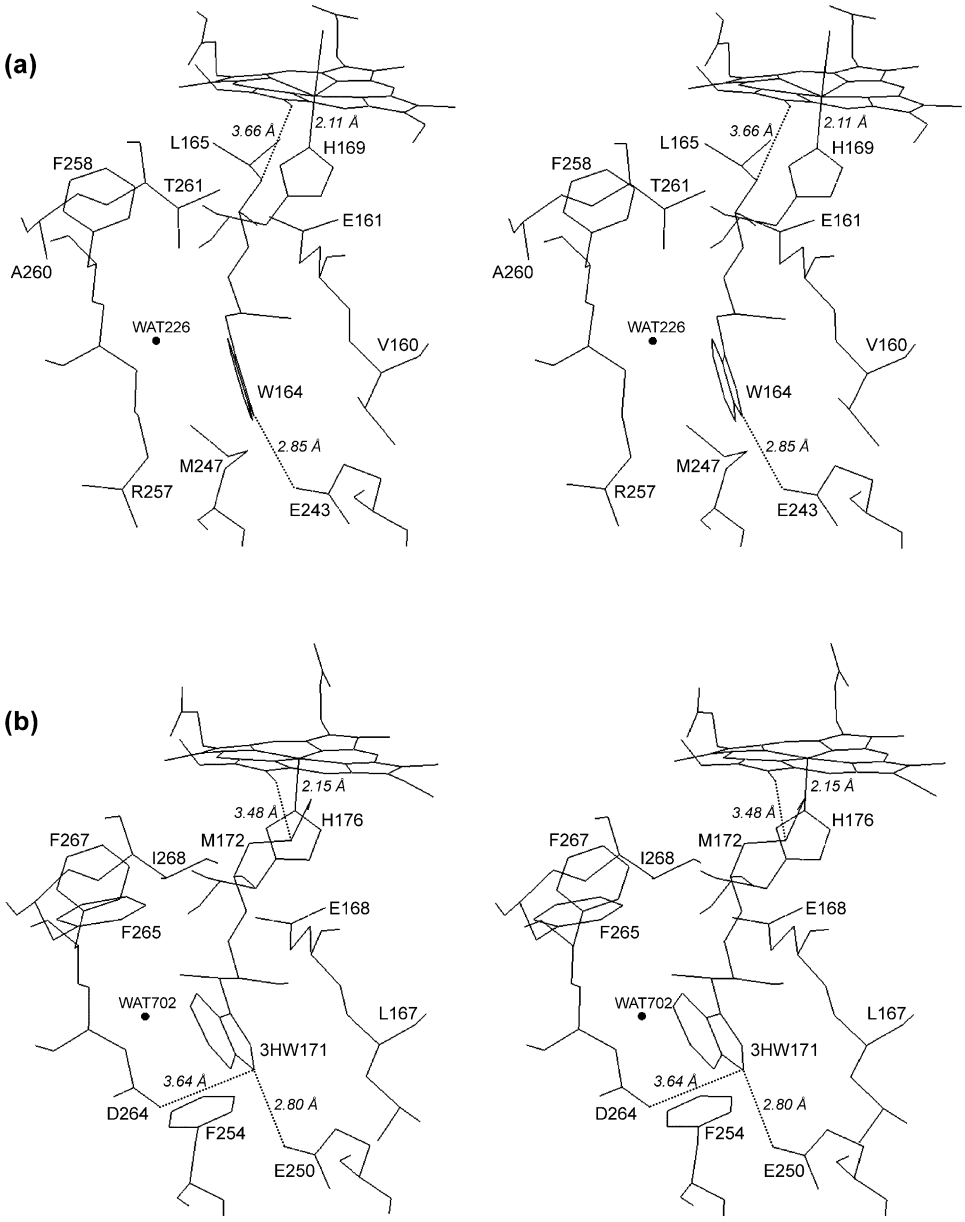

Figure 6. Stereo views of the exposed Trp involved in electron transfer to heme, and neighbor residues, in VP (a) and LiP (b) crystals. The crystal structures of native VP* (allelic variant VPL2) and wild-type LiP (isoenzyme H8) were solved at resolutions of 1.33 Å (PDB entry 2BOQ) and 1.70 Å (PDB entry 1LLP), respectively. The putative LRET pathway in VP would proceed from the solvent exposed Trp164 to Leu165, and from its C^{β} to the methyl of heme pyrrol-C at 3.66 Å. In the case of LiP the pathway would proceed from the solvent exposed Trp171 through Met172 to the heme methyl. Eight neighbor residues (and one water molecule) are shown to illustrate differences between both structures, as well as the proximal histidine resdiues, whose N^{ϵ} acts as ligand of heme iron. Among these residues VP Val160, Met247, Arg257, Ala260 and Thr261 occupy the positions of LiP Leu167, Phe254, Asp264, Phe265, Ile268, respectively, whereas VP Glu161, Glu243 and Phe258 are conserved in LiP as Glu168, Glu250 and Phe267.

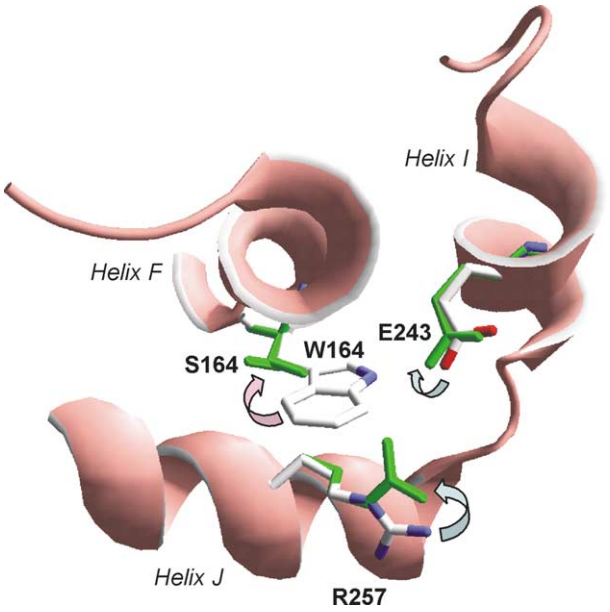

Figure 7. Superimposition of residues (Glu243 and Arg257) near Trp164 in native VP and the W164S variant crystal structures. Crystal structures of native VP* and its W164S variant were obtained at resolutions of 1.33 Å and 1.03 Å, respectively. The existence of two equally probable positions of Ser164 side-chain, and the displacement of Glu243 and Arg257 side-chains in the W164S variant with respect to the native VP* are indicated (arrows).

hydrogen bond with the side-chain of Glu243, which had slightly moved if compared to the situation in the native structure.

Discussion

VP substrate oxidation sites: SDM evaluation of LRET pathways

The wide substrate specificity of VP enzymes, which constitute a new family of peroxidases combining LiP, MnP and CIP catalytic properties,[7,44] suggests the existence of several binding sites accounting for its different activities.[33] A complete crystallographic characterization of the wild-type and recombinant VP at high resolution has been recently achieved (Piontek *et al.*, unpublished results). Moreover, the crystal structures of H_2O_2-treated VP* and the W164S variant are reported here at 1.03–1.33 Å resolution. Several putative substrate oxidation sites had been identified in VP, including a Mn^{2+} binding site similar to that found in MnP,[10] whose location and functionality were initially shown by NMR and site-directed mutagenesis.[45] However, additional studies are required, since the crystal structures described here suggest the involvement of Glu36 and Asp175, but shed some doubt on the involvement of Glu40 in Mn^{2+} oxidation by *P. eryngii* VP.

The two VP* crystal structures also show several residues potentially involved in the oxidation of veratryl alcohol and other aromatic compounds *via* two LRET pathways starting at VPL Trp164 and His232 that could form indole or imidazole side-chain radicals (Figure 8(a), I and II). Similar pathways had been proposed in *P. chrysosporium* LiP[14–16] together with a third LRET pathway (Figure 8(c), I–III).[6] The latter (pathway III) is absent from the crystal structure of the recombinant isoenzyme VPL, but is indicated from the homology model (PDB entry 1QJR) of isoenzyme VPS1,[32] starting at His82 (Figure 8(b), II and III). None of the above pathways (from exposed Trp or His residues) exist in the crystal structure of *P. chrysosporium* MnP (Figure 8(d)). The crystal structures show that the first residues of the above pathways are solvent accessible, situated at the protein surface. The pathways lengths in VP, 8–11 Å from the C^{α} of the exposed residue to the heme carbon atoms, is similar to those proposed in LiP H2 and H8.[14–16] Interestingly, a similar distance exists between the Trp191 C^{α} and the heme in the CCP crystal structure;[46] however, due to the orientation of the Trp side-chain the indole ring has a much closer distance of only 5 Å from the heme iron. Concerning the residues involved, a Pro residue in the two LiP isoenzymes occupies the position of VPL Ala77. Moreover, a Met in LiP-H8 occupies the position of VPL Leu165. However, this difference does not seem to be of significance to the LRET in the two isoenzymes, suggesting the C^{β} atom makes the contact to the heme edge.

Since the isoenzyme VPL only shows two of the LRET pathways described above, the mutations introduced included both: (i) removal of the surface residues of the two pathways present in VPL; and (ii) introduction of the third pathway present in VPS1 by mutation of the surface residue (in combination with removal of one of the others). The steady-state kinetics of the five variants obtained definitively show that only one of the three putative pathways investigated (pathway II) is operative for oxidation of the two high redox-potential substrates investigated, veratryl alcohol and Reactive Black 5. VP activity on these substrates is completely lost in the variants lacking Trp164, but is not affected by the removal or introduction of the two other pathways (I and III). Substitution of Trp164 either by Ser or His resulted in similar incapability of the enzyme to oxidize both compounds. The His imidazole side-chain is, therefore, not playing a similar role as the Trp indole moiety. This agrees with results reported for other radical proteins, where Trp and Tyr radicals are often detected by EPR and other techniques (see below), although His radicals have been suggested.[47] It is interesting that VP, as all known LiP and MnP proteins, does not include Tyr residues in its sequence (probably to prevent oxidative damage during the degradation of lignin) and that W164 is

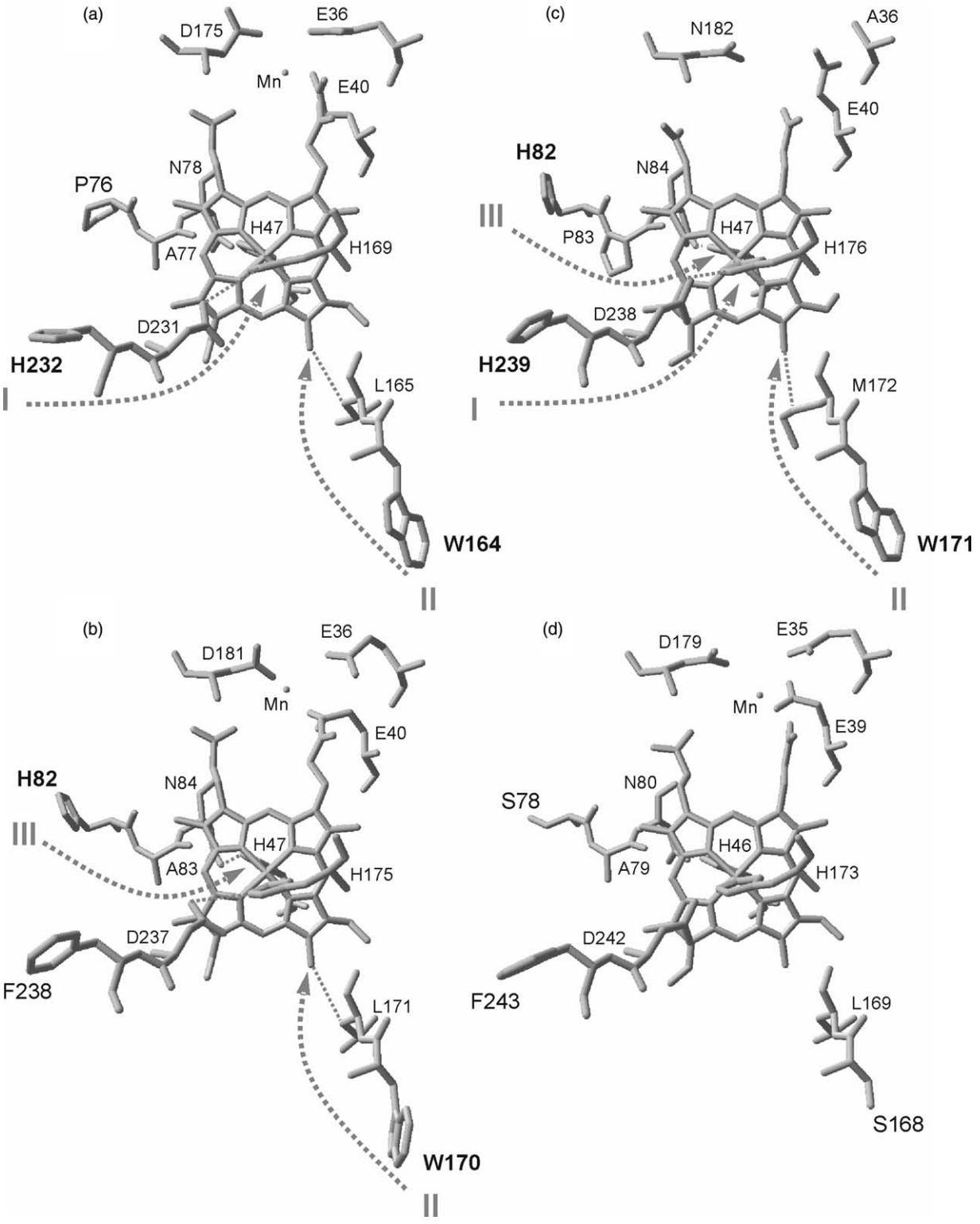

Figure 8. Putative LRET pathways in LiP and VP molecular structures. Axial view of the peroxidase heme (from proximal His side) showing LRET pathways in *P. eryngii* VP isoenzymes VPL (from solvent exposed Trp164 and His232) (a) and VPS1 (from exposed His82 and Trp170) (b), and *P. chrysosporium* LiP isoenzyme H8 (from exposed His82, Trp171 and His239) (c), and the corresponding amino acid residues in *P. chrysosporium* MnP isoenzyme 1 (d). Adapted from Ruiz-Dueñas *et al.*[44]

the only exposed Trp residue in VP despite that it has a second (internal) Trp.[22] The crystallographic study of the W164S variant shows that the substitution of the bulky Trp residue by a Ser caused a large conformational change of the Arg257 side-chain. The eventual influence of this second modification on the activity of this variant is still to be investigated.

Involvement of a tryptophan residue in VP catalysis had already been suggested after NBS bromination of *P. eryngii*, *Pleurotus ostreatus* and *Bjerkandera* sp. VP isoenzymes.[43,44,48,49] Recent cloning of the two latter peroxidases (GenBank code AJ243977 with 95% amino acid identity with VPS1, and AY217015 with 69% identity with VPL) has shown that both exhibit an exposed Trp homologous to VPL Trp164 as well as a putative Mn-binding site. The present results also support studies on the role of Trp171 in veratryl alcohol oxidation by LiP,[17,50,51] in contrast with some results suggesting oxidation at the classical heme channel entrance.[52] Pathway III has recently been investigated also in LiP[53] and the results are in agreement with those obtained for VP. Pathway I was proposed in LiP more recently than the two others putative pathways,[14] and its eventual role in catalysis has not been proved in this peroxidase using site-directed mutagenesis. Finally, it has been shown that a tetrameric lignin model compound is degraded by LiP but it is not oxidized by its W171S LiP variant.[54] This result suggests that polymeric lignin would be oxidized at the same exposed Trp residue involved in veratryl alcohol oxidation. However, this conclusion requires additional investigation using different lignin preparations (e.g. before and after permethylation of phenolic units), since it has been reported that a lignin dehydrogenation polymer (DHP) would bind LiP at His239.[14]

Tryptophanyl free radical in VP: proposal for a modified catalytic cycle

VP shares with LiP not only the ability to oxidize veratryl alcohol but also the spontaneous decay of the oxidized enzyme to its resting state, a process that is relatively rapid compared with other peroxidases.[17] The results from site-directed mutagenesis discussed above show that both VP properties are related, since the W164S variant: (i) was unable to oxidize veratryl alcohol; and (ii) its compound II was not self-reduced to the resting state as native VP* did. Both characteristics are very likely related to the formation of a free radical of the exposed Trp164 as discussed. Formation of a tryptophanyl radical was already suggested in H_2O_2-activated LiP,[51] but EPR signals of LiP compound I were previously assigned to a porphyrin π cation radical.[55] In the present study, formation of a protein radical in H_2O_2-activated VP could be demonstrated by EPR, in contrast with results reported in LiP but agreeing with recent results with *Bjerkandera adusta* VP.[43] Assignment of the protein radical EPR signal to a tryptophan radical is reinforced by the fact that tyrosine residues are absent from the amino acid sequence of VP, as mentioned above. Moreover, multifrequency EPR and electron nuclear double resonance (ENDOR) measurements and density functional theory (DFT) calculations (data not shown) confirmed the Trp164 radical in the *P. eryngii* VP*, and showed that it is in the neutral form. By contrast, the cation radical of Trp171 is generally postulated as the reactive form in LiP,[51] although its neutral radical has been suggested as an intermediate in the hydroxylation of Trp171 discussed below.[50]

As suggested by Doyle *et al.*[17] for LiP, the VP Trp164 radical is produced even in the absence of a substrate molecule. If this was not the case, as suggested in a different study:[53] (i) the decay of VP* compound I would not be affected in the W164S variant; and (ii) the tryptophanyl radical would not be detected by low temperature EPR in the absence of substrate. Interestingly, it was the reduction of compound II to the resting state that was completely blocked in the VP W164S variant, suggesting alternative mechanisms (e.g. a second electron transfer pathway from a different residue) for reduction of compound I (more reactive than compound II) in the absence of Trp164. This blockage has not been reported in LiP where, however, differences in compound I reduction kinetics are produced after removal of Trp171.[17] The two ligninolytic peroxidases (VP and LiP) are therefore included in the group of enzymes forming a Trp radical involved in catalysis, together with CCP and DNA photolyase.[3,56] In the well-known case of CCP, a proximal Trp, located close to the heme, is directly oxidized by the porphyrin cation-radical at the end of a LRET pathway transporting electrons from cytochrome *c*. In the two other cases, the Trp radical would be at the beginning of the LRET pathway receiving the electrons directly from an enzyme substrate. Finally, a Trp radical apparently not involved in catalysis has been described in ascorbate peroxidase after reaction with H_2O_2 in the absence of substrate.[57] Since this peroxidase has only two Trp residues, which are homologous to the distal and proximal CCP Trp51 and Trp191, it is most likely that the radical will be homologous to that formed in CCP albeit much less stable (formed only after long-term decay of the compound I porphyrin radical).

Taking the above results into account, the basic VP cycle (Figure 1(a)) proposed by Ruiz-Dueñas *et al.*[22] can be now completed for the part corresponding to the oxidation of veratryl alcohol, and other high redox potential substrates (Figure 1(b)). The modification proposed, which agrees with the mechanisms described for LiP,[17,50,51] implies the existence of two peroxidase forms, called compounds I_B and II_B by analogy with the names used for two forms of CCP compound II,[35] characterized because one oxidation equivalent would be in the form of a Trp radical. These two forms would be in equilibrium with the classical compounds I and II (now called compounds I_A and II_A), where the above oxidation equivalent is in the form of a porphyrin cation radical and a Fe^{4+}-oxo, respectively. The existence of two forms with the same number of oxidation equivalents has been described in the transient states of some peroxidases, such as prostaglandin H synthase compound

I and CCP compound II, among others.[35,58] In the case of VP, the percentage of each of forms A and B in the two equilibrium reactions could be variable, and its involvement in catalysis will depend on the substrates available. In other words the "classical" compounds I_A and II_A will be predominant during oxidation of Mn^{2+}, whereas a certain percentage of the protein radical forms will be necessary during oxidation of veratryl alcohol. The EPR results show that the VP Trp164 radical is present in the compound I equilibrium (representing around 25% under the experimental conditions used). The existence of compound II_B, that in CCP represents 10% of total compound II at pH 5,[58] is still to be directly demonstrated in VP, although its presence is required for catalysis as mentioned above.

Aromatic substrate oxidation: VP *versus* LiP

The results presented here support some of the most recent findings concerning aromatic substrate oxidation by ligninolytic peroxidases (LiP and VP). Namely, the essential role of an exposed Trp residue, and the formation of a redox active protein radical at this position. However, some significant differences exist in aromatic substrate oxidation between both ligninolytic peroxidases. One being the lack of hydroxylation of VP* Trp164 after treatment with H_2O_2, in contrast with the C^{β} hydroxylation found in the moiety of Trp171 both in the wild LiP-H8 produced by *P. chrysosporium* and in the recombinant enzyme from *E. coli* exposed to a few peroxide equivalents.[50,59,60] Since the resolution of the corresponding crystal structures was by far high enough to recognize a bound hydroxyl group, its absence there is definite. Furthermore, no C^{β}-hydroxylation at Trp164 was found in the crystal structure of fungal VP (data not shown). The functional relevance of this difference is being investigated.

In addition to the ability of VP to oxidize Mn^{2+} with similar efficiency as MnP, which obviously is not shared by LiP, there are still two important functional differences between VP and LiP. Despite both enzymes can oxidize veratryl alcohol at a similar rate, LiP exhibits a higher affinity for this substrate resulting in higher oxidation efficiency. On the other hand, VP is able to directly oxidize Reactive Black 5 and other dyes (as well as substituted phenols) that LiP oxidizes only in the presence of veratryl alcohol (Table 3). The results obtained here show that Trp164 is the oxidation site of at least one of these dyes (Reactive Black 5) in VP. Therefore, the above differences in enzyme catalysis could be related to differences in the environment of the exposed Trp residue in both enzymes (Figure 9). Trp171 in LiP isoenzymes is surrounded by four acidic residues (Glu168, Asp165, Glu250 and Glu264), whereas only two are present close to VPL Trp164 (Glu161 and Glu243). The more acidic environment could stabilize an intermediate veratryl alcohol cation radical increasing LiP affinity. This would also favor the function of the radical as an enzyme-bound mediator[61] in oxidation of some substrates that, by contrast, can be directly oxidized by VP. This hypothesis has to be confirmed, but site-directed mutagenesis results show that substitution of Arg257 (near Trp164) by an acidic residue confers to VP some LiP-type catalytic properties.

Table 3. Comparison of VP and LiP capabilities for the oxidation of some dyes

	Phthalocyanine dyes		Azo dyes	
	RB38	RB15	RV5	RB5
VP	6.7	7.7	5.8	3.9
LiP	0.6	0.9	0.2	0.2
LiP + VA	4.2	7.6	4.5	4.1

Turnover numbers (s^{-1}) for the oxidation of phthalocyanine (RB38, Reactive Blue 38; and RB15, Reactive Blue 15) and azo (RV5, Reactive Violet 5; and RB5, Reactive Black 5) dyes by VPL obtained from *P. eryngii* and LiP obtained from *B. adusta*. The reactions were carried out in 100 mM sodium tartrate (pH 3.5, azo dyes; or pH 3.75, phthalocyanine), and were initiated by adding 0.1 mM H_2O_2. Adapted from Heinfling *et al.*39

The high stability of the Trp cation radical in CCP has been attributed to the existence of an electronegative environment including an acidic residue (Asp235) at H-bond distance from the indole nitrogen atom.[46] It is interesting that a similar H-bond exists in both VP (Glu243..Trp164) and LiP (Glu250..Trp171), probably contributing to stabilize the radical of the active Trp residue (see Figure 6). This residue forms a second H-bond with a water molecule that is fully conserved in all VP and LiP (before and after H_2O_2 treatment) crystal structures. However, two important differences between the environment of the indole side-chain of the active Trp in VP and LiP concern the substitutions of LiP Phe254 and Asp264 by VP Met247 and Arg257, respectively. The first residue (Phe254) could establish aromatic interactions with Trp171 in LiP that would be absent in VP. Even more important, the carboxylate of the second residue (Asp264) forms a H-bond with the indole N of Trp171 and can contribute to further stabilization of the cation radical, together with the already mentioned Glu250. By contrast, the positively charged side-chain of Arg257 in VP would not stabilize a cation radical form of Trp164. Further investigations on these and other differences in the environment of the exposed Trp and LRET pathway will contribute to understand the mechanism of high redox potential aromatic substrate oxidation by ligninolytic peroxidases.

Conclusions

The present study provides the first information on the site and mechanism of oxidation of high redox potential aromatic substrates in VP, a peroxidase combining the catalytic properties of LiP, MnP and CIP. The availability of several crystal

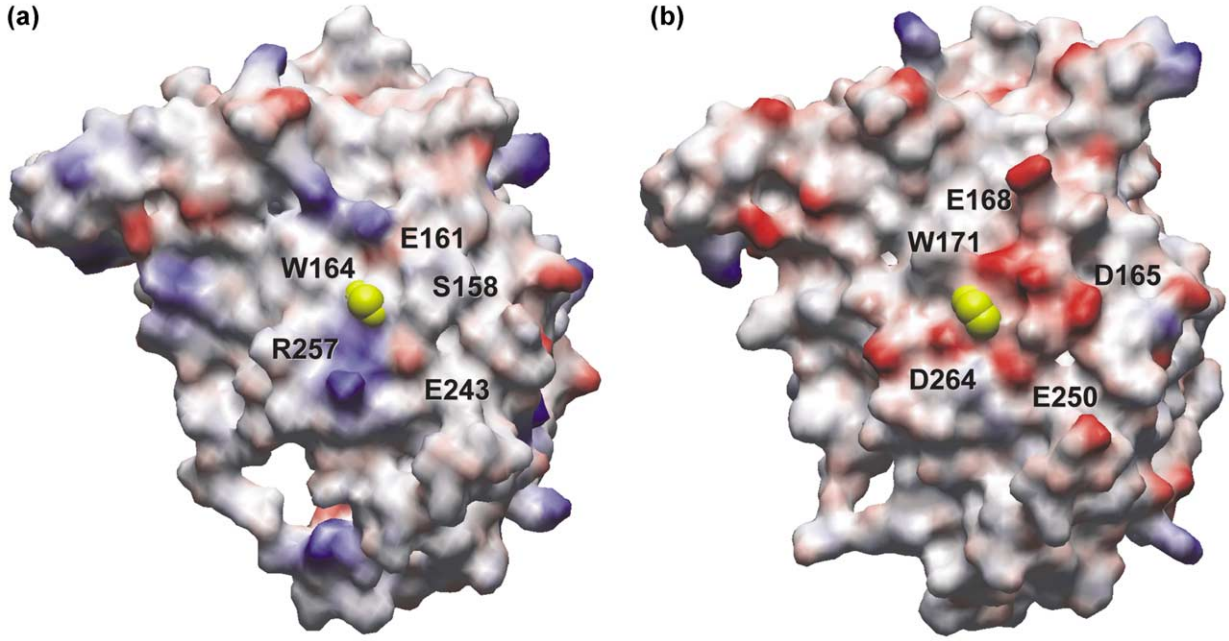

Figure 9. Comparison of solvent exposed residues surrounding Trp164 in the VP crystal structure (a), and homologous Trp171 in the LiP-H8 crystal structure (b). From PDB entries 2BOQ and 1LLP corresponding to native VP* (allelic variant VPL2) and wild-type LiP (isoenzyme H8), respectively. Four acidic residues are indicated around LiP Trp171 (in yellow) that contribute to the surface negative charge (in red), whereas only two acidic residues are present around VP Trp164 (in yellow) that is more basic (blue) than the same surface region in LiP.

structures and homology models of *P. eryngii* VP isoenzymes allowed identification of three possible LRET pathways. These three pathways were investigated using site-directed mutagenesis of exposed amino acid residues in isoenzyme VPL. The results show that only the pathway starting at Trp164 was operational in oxidation of two model aromatic substrates by VP. The VP LRET pathways are similar to those proposed for veratryl alcohol oxidation in *P. chrysosporium* LiP, although only two of them have been included in LiP site-directed mutagenesis studies.

Concerning oxidation mechanisms, we provide the first direct experimental data on the formation of a Trp radical in a ligninolytic peroxidase using low-temperature EPR of H_2O_2-activated VP. This result contrasts with previous EPR studies of LiP, and supports evidence on the formation of a Trp radical in the catalytic cycle of this peroxidase. Additional spectroscopic and DFT studies in course confirm the radical at Trp164 in the above LRET pathway and suggest it exists in the neutral form. Additional spectroscopic studies of the W164S variant suggested that the Trp164 radical is also involved in VP self-reduction after H_2O_2 activation. Although involvement of the homologous Trp residue in LiP self-reduction had been already suggested, we show here for the first time that its absence blocks self-reduction at the level of compound II. The VP crystallographic studies also revealed that the C^{β} of Trp164 is not hydroxylated in the wild-type VP nor in the pristine VP* treated with H_2O_2. This constitutes a variation with respect to LiP, and suggests differences in residues contributing to the stabilization of the Trp radical. Two additional differences, namely LiP higher affinity for veratryl alcohol and VP ability to directly oxidize high redox potential dyes, are currently under investigation, since they seem to be related to variations in the environment of the catalytically active Trp residue.

Materials and Methods

cDNA cloning

The cDNA encoding the mature sequence of *P. eryngii* VP (allelic variant VPL2; GenBank code AF007222)[22] was cloned in the expression vector pFLAG1 and the resulting plasmid pFLAG1-VPL2 was used for polymerase chain reaction (PCR) site-directed mutagenesis. *E. coli* W3110 was transformed with the plasmids containing the wild-type and mutated gene, and the VP* protein was obtained and activated *in vitro* as described below.

Site-directed mutagenesis

The mutations were introduced by PCR using the expression plasmid pFLAG1-VPL2 as template, and two primer design strategies. W164H, H232F, P76H and W164S/P76H mutations were introduced using the QuikChange™ Site-Directed Mutagenesis kit (Stratagene). For each mutation, both a direct and a reverse primer were designed complementary to opposite strands of

the same DNA region. Oligonucleotide sequences were as follows (mutated codons are shown in bold italics): W164H direct primer, 5′-CCCGTCGAGGTTGTT***CA C***CTCCTGGCTTCGCACTCC-3′; W164H reverse primer, 5′-GGAGTGCGAAGCCAGGAG***GTG***AACAACCTCG ACGGG-3′; H232F direct primer, 5′-GGCTTCAGTCC GAT***TTC***TTGTTGGCTAGAGACCCC-3′; H232F reverse primer, 5′-GGGGTCTCTAGCCAACAA***GAA***ATCGG ACTGAAGCC-3′; P76H direct primer, 5′-CCATTGA GACTAATTTC***CAC***GCCAATGCTGGCATCG-3′; P76H reverse primer, 5′-CGATGCCAGCATTGGC***GTG*** GAAATTAGTCTCAATGG-3′. The double mutant W164S/P76H was obtained as described for the single ones but using plasmid pFLAG1-VPL2(W164S) as template and direct and reverse oligonucleotides for mutation P76H as primers. Clones harboring mutations were transformed into *E. coli* DH5α. One positive clone of each mutant was completely sequenced (Perkin-Elmer ABI PRISM 377) and used to transform *E. coli* W3110.

A different mutagenesis method[17] was also assayed, and used to introduce the W164S mutation. This is based on generation of a new restriction site after PCR amplification only when the ligation event produced an intact gene. For this purpose, two primers were designed: the mutagenic primer (5′-C**C**GCAATGGAGTGCGA AGCCAGGAG ***CGA***AAC-3′), which overlapped the area to be mutated (in bold italics); and the reference primer (5′ C**C**GCCGACAAGGTTGACC 3′) which annealed to the other DNA strand. Both primers coincided exactly back-to-back on opposite strands of the template DNA, pFLAG1-VPL2, and contained a silent mutation (underlined and bold) at their 5′ end to create a new NotI restriction site unique to the plasmid. After amplification, a linear DNA fragment was obtained identical in size to linearized pFLAG1-VPL2, which was cleaned by gel extraction (Geneclean II, BIO101 Inc.), phosphorylated using T4 polynucleotide kinase, ligated using T4 DNA ligase and transformed into *E. coli* DH5α. Positive colonies were selected on the basis of digestion of their plasmidic DNA by NotI, thus excluding wild-type plasmids and mutant plasmids bearing deletions due to spurious exonuclease activity of polymerase. After complete automated sequencing, one of the positive clones was used to transform *E. coli* W3110.

PCR reactions were carried out in a Perkin-Elmer Gene Amp PCR system 240 using 10 ng of template DNA, 250 μM each dNTP, 125 ng of mutagenic and reference primers or direct and reverse primers, 2.5 units of *Pfu*Turbo polymerase (Stratagene), and the manufacture's reaction buffer. Reaction conditions were as follows: (i) a "hot start" of 95 °C for 1 min; (ii) 18 cycles at 95 °C for 50 s, 55 °C for 50 s and 68 °C for 10 min; and (iii) a final cycle at 68 °C for 10 min.

Enzyme production, activation and purification

Native VP* protein and its site-directed mutagenesis variants were produced in *E. coli* W3110 after transformation with the corresponding plasmids.[34] Cells were grown for 3 h in Terrific Broth,[62] induced with 1 mM isopropyl-β-D-thiogalactopyranoside (IPTG), and grown for a further 4 h. The apoenzyme accumulated in inclusion bodies, as shown by SDS-PAGE, and was recovered using 8 M urea. Subsequent *in vitro* folding was performed using 0.15 M urea, 5 mM Ca^{2+}, 20 μM hemin, a 5:1 oxidized-glutathione/dithiothreitol ratio, and 0.1 mg/ml protein concentration, at pH 9.5.[34] Active enzyme was purified by Mono-Q chromatography using a 0–0.3 M NaCl gradient (2 ml/min, 20 min) in 10 mM sodium tartrate (pH 5.5) supplemented with 1 mM $CaCl_2$.

Enzymatic activities

Direct oxidation of Mn^{2+} was estimated by the formation of a Mn^{3+} tartrate complex (ε_{238} 6500 M^{-1} cm^{-1}) using 100 mM sodium tartrate (pH 5) and 0.1 mM $MnSO_4$. Mn-independent activities on 2 mM veratryl alcohol (veratraldehyde ε_{310} 9300 M^{-1} cm^{-1}) was estimated at pH 3.0, and on 0.1 mM Reactive Black 5 (ε_{598} 30, 000 M^{-1} cm^{-1}) at pH 3.5. All enzymatic activities were measured as initial velocities taking linear increments (decreases in the case of the azo dye Reactive Black 5) at 24 °C in the presence of 0.1 mM H_2O_2 using a Shimadzu UV-160 spectrophotometer.

Enzyme kinetics

Steady-state kinetic constants were calculated from the estimated oxidation of increasing substrate concentrations at 24 °C until enzyme saturation was observed. Values and standard errors for apparent affinity constant (K_m) and maximal enzyme turnover (k_{cat}) were obtained fitting the experimental measurements to the Michaelis–Menten model by double-reciprocal plots, using the SIMFIT software application. Fitting of these constants to a normalized Michaelis–Menten equation defined as $v=(k_{cat}/K_m)[S]/(1+[S]/K_m)$ yielded enzyme efficiency values (k_{cat}/K_m) with their corresponding standard errors.

Transient-state kinetic constants of compound I formation (k_1) by H_2O_2 (followed at 397 nm) and compound II formation (k_2) and reduction (k_3) by veratryl alcohol were investigated (at 426 nm) in 20 mM sodium tartrate at 24 °C and different pH values using an Applied Photophysics stopped-flow spectrophotometer equipped with a diode-array detector, and the corresponding software. Taking advantage from the high speed of the VP* reaction with H_2O_2 compared with the reaction with veratryl alcohol, k_2 and k_3 were estimated by an one-step mixing procedure.

Spectroscopic measurements

Electronic absorption spectra were recorded at 24 °C using a variable wavelength Shimadzu UV-160 and a diode-detector Hewlett-Packard 8453 spectrophotometers. The concentrations of native VP* and site-directed mutagenesis variants were calculated from the absorption at 407 nm of their resting state spectra using an extinction coefficient of 150 mM^{-1} cm^{-1}.[22] For spectroscopic characterization of the transient states in VP catalytic cycle, one or two equivalents of H_2O_2 were added to the resting enzyme in 10 mM sodium tartrate (pH 5), yielding compounds I and II, respectively.[36,37] Long-term self-reduction of compound I (prepared as described above) was followed in the 375 nm–475 nm range using only the visible lamp of the diode-array spectrophotometer (to prevent UV photoreduction).

EPR measurements were performed in solutions containing 0.16 mM VP* and 1.3 mM H_2O_2 in 0.1 M phthalate buffer (pH 4.5). The reaction was stopped by rapid immersion of the EPR tube in liquid nitrogen after 10 s. CW-X-band (9 GHz) EPR measurements were carried out with a Bruker E500 Elexsys Series using

Table 4. Statistics of data collection and processing, and refinement

A. *Data collection and processing*			B. *Refinement*		
	VP*-H_2O_2	W164S		VP*-H_2O_2	W164S
Beamline	SLS/X06SA	SLS/X06SA	Resolution range (Å)	1.33–63	1.03–60
λ (Å)	0.91839	0.91839	R_{cryst}/R^*_{free} (%)	15.9/18.2	13.1/14.5
T (K)	100	100	Bond rmsd (Å)	0.016	0.022
Unit –cell *a* (Å)	62.80	63.20	Molecules	1	1
Unit –cell *b* (Å)	62.80	63.20	Residues	1–319	1–320
Unit –cell *c* (Å)	98.22	99.24	Heteroatoms	2 Ca^{2+} +5 Zn^{2+} +1 Mn^{2+}	2 Ca^{2+} +5 Zn^{2+}
Resolution range (Å)	1.33–65	1.03–65	Cofactor	1 heme	1 heme
Completeness (%)	99.6	97.6	Solvent atoms	377	547
R_{sym} (%)	8.6	9.7			
I/σ	10.4	12.0			

the Bruker ER 4122 SHQE cavity and an Oxford helium continuous flow cryostat (ESR900).

Crystallization, data collection, and crystal structure determination

A detailed description of VP crystallization and crystal structure determination will be provided elsewhere (Piontek *et al.*, unpublished results). Native VP* (allelic variant VPL2) was incubated with six equivalents of H_2O_2, in the absence of an enzyme-reducing substrate, prior to crystallization. Initial crystallization conditions of peroxide-treated VP* and the W164S variant were found by employing a commercial screen (Hampton Research) using the hanging drop vapor diffusion method, and were subsequently improved by varying different parameters.

For native VP* the optimized crystallization conditions were the following: 9.0 mg/ml protein (in 10 mM sodium tartrate (pH 5.5)) in 100 mM sodium cacodylate (pH 6.5), containing 200 mM Zn-acetate and 17% polyethylene glycol (PEG) 10000. For the W164S variant the conditions differed only in the sodium cacodylate pH (5.0), Zn-acetate concentration (100 mM), and use of 14% PEG 8000. The activity of re-dissolved crystals was tested confirming that no iron loss took place.

Cryo-conditions were established before final data collection at a synchrotron source. Diffraction data were collected at the X06SA beam line of the Swiss Light Source (SLS) synchrotron at 100 K applying the oscillation method. Diffraction data were processed and scaled with the program package XDS/XSCALE.[63] The two isomorphous crystal structures were solved employing the molecular replacement technique with the program AMoRe,[64] using the LiP-H2 crystal structure (PDB entry 1QPA) as search model. Refinement of the initial models with the program REFMAC from the CCP4 suite[65] and subsequent rounds of rebuilding using various omit difference maps resulted in well defined structures. The statistics of crystallographic data collection, processing and refinement are summarized in Table 4.

Protein Data Bank accession numbers

The atomic coordinates and structure factors of H_2O_2 pretreated native VP* have been deposited in the Protein Data Bank, Research Collaboratory for Structural Bioinformatics, Rutgers University, New Brunswick, NJ, with accession code 2BOQ.

Acknowledgements

This research was supported by EU contract QLK3-99-590, and the Spanish Biotechnology project BIO2002-1166. The authors thank Dr A. T. Smith (University of Sussex, UK) for valuable comments and help. M.P.-B. thanks the Spanish Ministry of Science and Technology (MCyT) for an FPI Fellowship, and F.J.R.-D. thanks the CSIC for an I3P contract. The use of the protein beam line at the SLS synchrotron (Villigen, Switzerland) is gratefully acknowledged.

References

1. Beratan, D. N., Onuchic, J. N., Winkler, J. R. & Gray, H. B. (1992). Electron-tunneling pathways in proteins. *Science*, **258**, 1740–1741.
2. Pelletier, H. & Kraut, J. (1992). Crystal structure of a complex between electron transfer partners, cytochrome *c* peroxidase and cytochrome *c*. *Science*, **258**, 1748–1755.
3. Aubert, C., Mathis, P., Eker, A. P. & Brettel, K. (1999). Intraprotein electron transfer between tyrosine and tryptophan in DNA photolyase from *Anacystis nidulans*. *Proc. Natl Acad. Sci. USA*, **96**, 5423–5427.
4. Kirk, T. K. & Farrell, R. L. (1987). Enzymatic "combustion": the microbial degradation of lignin. *Annu. Rev. Microbiol.* **41**, 465–505.
5. Harvey, P. J. & Palmer, J. M. (1990). Oxidation of phenolic compounds by ligninase. *J. Biotechnol.* **13**, 169–179.
6. Schoemaker, H. E., Lundell, T. K., Floris, R., Glumoff, T., Winterhalter, K. H. & Piontek, K. (1994). Do carbohydrates play a role in lignin peroxidase cycle? Redox catalysis in the endergonic region of the driving force. *Bioorg. Med. Chem.* **2**, 509–519.
7. Martínez, A. T. (2002). Molecular biology and structure–function of lignin-degrading heme peroxidases. *Enzyme Microb. Technol.* **30**, 425–444.
8. Smith, A. T. & Veitch, N. C. (1998). Substrate binding and catalysis in heme peroxidases. *Curr. Opin. Chem. Biol.* **2**, 269–278.
9. Banci, L. (1997). Structural properties of peroxidases. *J. Biotechnol.* **53**, 253–263.
10. Gold, M. H., Youngs, H. L. & Gelpke, M. D. (2000). Manganese peroxidase. *Met. Ions Biol. Syst.* **37**, 559–586.

11. Henriksen, A., Schuller, D. J., Meno, K., Welinder, K. G., Smith, A. T. & Gajhede, M. (1998). Structural interactions between horseradish peroxidase C and the substrate benzhydroxamic acid determined by X-ray crystallography. *Biochemistry*, **37**, 8054–8060.
12. Itakura, H., Oda, Y. & Fukuyama, K. (1997). Binding mode of benzhydroxamic acid to *Arthromyces ramosus* peroxidase shows by X-ray crystallographic analysis of the complex at 1.6 Å resolution. *FEBS Letters*, **412**, 107–110.
13. Harvey, P. J., Schoemaker, H. E. & Palmer, J. M. (1986). Veratryl alcohol as a mediator and the role of radical cations in lignin biodegradation by *Phanerochaete chrysosporium*. *FEBS Letters*, **195**, 242–246.
14. Johjima, T., Itoh, H., Kabuto, M., Tokimura, F., Nakagawa, T., Wariishi, H. & Tanaka, H. (1999). Direct interaction of lignin and lignin peroxidase from *Phanerochaete chrysosporium*. *Proc. Natl Acad. Sci. USA*, **96**, 1989–1994.
15. English, A. M. & Tsaprailis, G. (1995). Catalytic and structure–function relationships in heme proteins. *Advan. Inorg. Chem.* **43**, 79–125.
16. Du, P., Collins, J. R. & Loew, G. H. (1992). Homology modeling of a heme protein, lignin peroxidase, from the crystal structure of cytochrome *c* peroxidase. *Protein Eng.* **5**, 679–691.
17. Doyle, W. A., Blodig, W., Veitch, N. C., Piontek, K. & Smith, A. T. (1998). Two substrate interaction sites in lignin peroxidase revealed by site-directed mutagenesis. *Biochemistry*, **37**, 15097–15105.
18. Martínez, D., Larrondo, L. F., Putnam, N., Gelpke, M. D., Huang, K., Chapman, J. *et al*. (2004). Genome sequence of the lignocellulose degrading fungus *Phanerochaete chrysosporium* strain RP78. *Nature Biotechnol.* **22**, 695–700.
19. Baunsgaard, L., Dalboge, H., Houen, G., Rasmussen, E. M. & Welinder, K. G. (1993). Amino acid sequence of Coprinus macrorhizus peroxidase and cDNA sequence encoding *Coprinus cinereus* peroxidase–a new family of fungal peroxidases. *Eur. J. Biochem.* **213**, 605–611.
20. Mester, T. & Field, J. A. (1998). Characterization of a novel manganese peroxidase-lignin peroxidase hybrid isozyme produced by *Bjerkandera* species strain BOS55 in the absence of manganese. *J. Biol. Chem.* **273**, 15412–15417.
21. Martínez, M. J., Ruiz-Dueñas, F. J., Guillén, F. & Martínez, A. T. (1996). Purification and catalytic properties of two manganese-peroxidase isoenzymes from *Pleurotus eryngii*. *Eur. J. Biochem.* **237**, 424–432.
22. Ruiz-Dueñas, F. J., Martínez, M. J. & Martínez, A. T. (1999). Molecular characterization of a novel peroxidase isolated from the ligninolytic fungus *Pleurotus eryngii*. *Mol. Microbiol.* **31**, 223–236.
23. Camarero, S., Böckle, B., Martínez, M. J. & Martínez, A. T. (1996). Manganese-mediated lignin degradation by *Pleurotus pulmonarius*. *Appl. Environ. Microbiol.* **62**, 1070–1072.
24. Sarkar, S., Martínez, A. T. & Martínez, M. J. (1997). Biochemical and molecular characterization of a manganese peroxidase isoenzyme from *Pleurotus ostreatus*. *Biochim. Biophys. Acta*, **1339**, 23–30.
25. Martínez, M. J. & Martínez, A. T. (1996). Characterization of MnP isoenzymes of *Pleurotus eryngii* exhibiting Mn-independent activities on 2,6-dimethoxyphenol and veratryl alcohol. In *Biotechnology in the Pulp and Paper Industry: Recent Advances in Applied and Fundamental Research* (Messner, K. & Srebotnik, E., eds), pp. 417–420, Facultas-Universitätsverlag, Vienna.
26. Heinfling, A., Martínez, M. J., Martínez, A. T., Bergbauer, M. & Szewzyk, U. (1998). Purification and characterization of peroxidases from the dye-decolorizing fungus *Bjerkandera adusta*. *FEMS Microbiol. Letters*, **165**, 43–50.
27. Zorn, H., Langhoff, S., Scheibner, M., Nimtz, M. & Berger, R. G. (2003). A peroxidase from *Lepista irina* cleaves β,β-carotene to flavor compounds. *Biol. Chem.* **384**, 1049–1056.
28. Lisov, A. V., Leontievsky, A. A. & Golovleva, L. A. (2003). Hybrid Mn-peroxidase from the ligninolytic fungus *Panus tigrinus* 8/18. Isolation, substrate specificity, and catalytic cycle. *Biochemistry (Moscow)*, **68**, 1027–1035.
29. Welinder, K. G. (1992). Superfamily of plant, fungal and bacterial peroxidases. *Curr. Opin. Struct. Biol.* **2**, 388–393.
30. Caramelo, L., Martínez, M. J. & Martínez, A. T. (1999). A search for ligninolytic peroxidases in the fungus *Pleurotus erygnii* involving α-keto-γ-thiomethylbutyric acid and lignin model dimers. *Appl. Environ. Microbiol.* **65**, 916–922.
31. Heinfling, A., Ruiz-Dueñas, F. J., Martínez, M. J., Bergbauer, M., Szewzyk, U. & Martínez, A. T. (1998). A study on reducing substrates of manganese-oxidizing peroxidases from *Pleurotus eryngii* and *Bjerkandera adusta*. *FEBS Letters*, **428**, 141–146.
32. Camarero, S., Ruiz-Dueñas, F. J., Sarkar, S., Martínez, M. J. & Martínez, A. T. (2000). The cloning of a new peroxidase found in lignocellulose cultures of *Pleurotus eryngii* and sequence comparison with other fungal peroxidases. *FEMS Microbiol. Letters*, **191**, 37–43.
33. Camarero, S., Sarkar, S., Ruiz-Dueñas, F. J., Martínez, M. J. & Martínez, A. T. (1999). Description of a versatile peroxidase involved in natural degradation of lignin that has both Mn-peroxidase and lignin-peroxidase substrate binding sites. *J. Biol. Chem.* **274**, 10324–10330.
34. Pérez-Boada, M., Doyle, W. A., Ruiz-Dueñas, F. J., Martínez, M. J., Martínez, A. T. & Smith, A. T. (2002). Expression of *Pleurotus eryngii* versatile peroxidase in *Escherichia coli* and optimisation of *in vitro* folding. *Enzyme Microb. Technol.* **30**, 518–524.
35. Dunford, H. B. (1999). *Heme Peroxidases*, Wiley-VCH, New York.
36. Wariishi, H., Akileswaran, L. & Gold, M. H. (1988). Manganese peroxidase from the basidiomycete *Phanerochaete chrysosporium*: spectral characterization of the oxidized states and the catalytic cycle. *Biochemistry*, **27**, 5365–5370.
37. Renganathan, V. & Gold, M. H. (1986). Spectral characterization of the oxidized states of lignin peroxidase, an extracellular heme enzyme from the white rot basidiomycete *Phanerochaete chrysosporium*. *Biochemistry*, **25**, 1626–1631.
38. Schoemaker, H. E., Lundell, T. K., Hatakka, A. I. & Piontek, K. (1994). The oxidation of veratryl alcohol, dimeric lignin models and lignin by lignin peroxidase—the redox cycle revisited. *FEMS Microbiol. Rev.* **13**, 321–332.
39. Heinfling, A., Martínez, M. J., Martínez, A. T., Bergbauer, M. & Szewzyk, U. (1998). Transformation of industrial dyes by manganese peroxidase from *Bjerkandera adusta* and *Pleurotus eryngii* in a manganese-independent reaction. *Appl. Environ. Microbiol.* **64**, 2788–2793.

40. Zille, A., Ramalho, P., Tzanov, T., Millward, R., Aires, V., Cardoso, M. H. *et al*. (2004). Predicting dye biodegradation from redox potentials. *Biotechnol. Prog.* **20**, 1588–1592.
41. Smulevich, G. (1998). Understanding heme cavity structure of peroxidases: comparison of electronic absorption and resonance Raman spectra with crystallographic results. *Biospectroscopy*, **4**, S3–S17.
42. Bleifuss, G., Kolberg, M., Potsch, S., Hofbauer, W., Bittl, R., Lubitz, W. *et al*. (2001). Tryptophan and tyrosine radicals in ribonucleotide reductase: a comparative high-field EPR study at 94 GHz. *Biochemistry*, **40**, 15362–15368.
43. Pogni, R., Baratto, M. C., Giansanti, S., Teutloff, C., Verdin, J., Valderrama, B. *et al*. (2005). Tryptophan-based radical in the catalytic mechanism of versatile peroxidase from *Bjerkandera adusta*. *Biochemistry*, **44**, 4267–4274.
44. Ruiz-Dueñas, F. J., Camarero, S., Pérez-Boada, M., Martínez, M. J. & Martínez, A. T. (2001). A new versatile peroxidase from *Pleurotus*. *Biochem. Soc. Trans.* **29**, 116–122.
45. Banci, L., Camarero, S., Martínez, A. T., Martínez, M. J., Pérez-Boada, M., Pierattelli, R. & Ruiz-Dueñas, F. J. (2003). NMR study of Mn(II) binding by the new versatile peroxidase from the white-rot fungus *Pleurotus eryngii*. *J. Biol. Inorg. Chem.* **8**, 751–760.
46. Poulos, T. L. & Kraut, J. (1980). The stereochemistry of peroxidase catalysis. *J. Biol. Chem.* **255**, 8199–8205.
47. Boussac, A., Zimmermann, J. L., Rutherford, A. W. & Lavergne, J. (1990). Histidine oxidation in the oxygen-evolving photosystem-II enzyme. *Nature*, **347**, 303–306.
48. Kamitsuji, H., Watanabe, T., Honda, Y. & Kuwahara, M. (2004). Direct oxidation of polymeric substrates by multifunctional manganese peroxidase isozyme from *Pleurotus ostreatus* without redox mediators. *Biochem. J.* **386**, 387–393.
49. Ayala-Aceves, M., Baratto, M. C., Basosi, R., Vázquez-Duhalt, R. & Pogni, R. (2001). Spectroscopic characterization of a manganese-lignin peroxidase hybrid isozyme produced by *Bjerkandera adusta* in the absence of manganese: evidence of a protein centred radical by hydrogen peroxide. *J. Mol. Catal. B: Enzym.* **16**, 159–167.
50. Blodig, W., Doyle, W. A., Smith, A. T., Winterhalter, K., Choinowski, T. H. & Piontek, K. (1998). Autocatalytic formation of hydroxy group at Cβ of Trp171 in lignin peroxidase. *Biochemistry*, **37**, 8832–8838.
51. Blodig, W., Smith, A. T., Winterhalter, K. & Piontek, K. (1999). Evidence from spin-trapping for a transient radical on tryptophan residue 171 of lignin peroxidase. *Arch. Biochem. Biophys.* **370**, 86–92.
52. Ambert-Balay, K., Fuchs, S. M. & Tien, M. (1998). Identification of the veratryl alcohol binding site in lignin peroxidase by site-directed mutagenesis. *Biochem. Biophys. Res. Commun.* **251**, 283–286.
53. Gelpke, M. D. S., Lee, J. & Gold, M. H. (2002). Lignin peroxidase oxidation of veratryl alcohol: effects of the mutants H82A, Q222A, W171A, and F267L. *Biochemistry*, **41**, 3498–3506.
54. Mester, T., Ambert-Balay, K., Ciofi-Baffoni, S., Banci, L., Jones, A. D. & Tien, M. (2001). Oxidation of a tetrameric nonphenolic lignin model compound by lignin peroxidase. *J. Biol. Chem.* **276**, 22985–22990.
55. Khindaria, A. & Aust, S. D. (1996). EPR detection and characterization of lignin peroxidase porphyrin π-cation radical. *Biochemistry*, **35**, 13107–13111.
56. Sivaraja, M., Goodin, D. B., Smith, M. & Hoffman, B. M. (1989). Identification by ENDOR of Trp191 as the free-radical site in cytochrome-*c* peroxidase compound ES. *Science*, **245**, 738.
57. Hiner, A. N. P., Martínez, J. I., Arnao, M. B., Acosta, M., Turner, D. D., Raven, E. L. & Rodríguez-López, J. N. (2001). Detection of a tryptophan radical in the reaction of ascorbate peroxidase with hydrogen peroxide. *Eur. J. Biochem.* **268**, 3091–3098.
58. Ho, P. S., Hoffman, B. M., Kang, C. H. & Margoliash, E. (1983). Control of the transfer of oxidizing equivalents between heme iron and free radical site in yeast cytochrome *c* peroxidase. *J. Biol. Chem.* **258**, 4356–4363.
59. Blodig, W., Smith, A. T., Doyle, W. A. & Piontek, K. (2001). Crystal structures of pristine and oxidatively processed lignin peroxidase expressed in *Escherichia coli* and of the W171F variant that eliminates the redox active tryptophan 171. Implications for the reaction mechanism. *J. Mol. Biol.* **305**, 851–861.
60. Choinowski, T., Blodig, W., Winterhalter, K. & Piontek, K. (1999). The crystal structure of lignin peroxidase at 1.70 Å resolution reveals a hydroxyl group on the C^{β} of tryptophan 171: a novel radical site formed during redox cycle. *J. Mol. Biol.* **286**, 809–827.
61. Khindaria, A., Yamazaki, I. & Aust, S. D. (1996). Stabilization of the veratryl alcohol cation radical by lignin peroxidase. *Biochemistry*, **35**, 6418–6424.
62. Sambrook, J. & Russell, D. W. (2001). *Molecular Cloning*, CSHL Press, Cold Spring Harbor, New York.
63. Kabsch, W. (1993). Automatic processing of rotation diffraction data from crystals of initially unknown symmetry and cell constants. *J. Appl. Crystallog.* **26**, 795–800.
64. Navaza, J. (1994). AMoRe–an automated package for molecular replacement. *Acta Crystallog. sect. A*, **50**, 157–163.
65. Collaborative Computational Project No. 4. (1994). The CCP4 suite: programs from protein crystallography. *Acta Crystallog. sect. D*, **50**, 760–763.

Edited by M. Guss

(Received 1 July 2005; received in revised form 9 September 2005; accepted 16 September 2005)
Available online 3 October 2005